

# Conformational states control Lck switching between free and confined diffusion modes in T cells

Hilzenrat, Geva; Pandžić, Elvis; Yang, Zhengmin; Nieves, Daniel J.; Goyette, Jesse; Rossy, Jérémie; Ma, Yuanqing; Gaus, Katharina

DOI:

[10.1016/j.bpj.2020.01.041](https://doi.org/10.1016/j.bpj.2020.01.041)

License:

Creative Commons: Attribution-NonCommercial-NoDerivs (CC BY-NC-ND)

*Document Version*

Peer reviewed version

*Citation for published version (Harvard):*

Hilzenrat, G, Pandžić, E, Yang, Z, Nieves, DJ, Goyette, J, Rossy, J, Ma, Y & Gaus, K 2020, 'Conformational states control Lck switching between free and confined diffusion modes in T cells', *Biophysical Journal*, vol. 118, no. 6, pp. 1489-1501. <https://doi.org/10.1016/j.bpj.2020.01.041>

[Link to publication on Research at Birmingham portal](#)

## General rights

Unless a licence is specified above, all rights (including copyright and moral rights) in this document are retained by the authors and/or the copyright holders. The express permission of the copyright holder must be obtained for any use of this material other than for purposes permitted by law.

- Users may freely distribute the URL that is used to identify this publication.
- Users may download and/or print one copy of the publication from the University of Birmingham research portal for the purpose of private study or non-commercial research.
- User may use extracts from the document in line with the concept of 'fair dealing' under the Copyright, Designs and Patents Act 1988 (?)
- Users may not further distribute the material nor use it for the purposes of commercial gain.

Where a licence is displayed above, please note the terms and conditions of the licence govern your use of this document.

When citing, please reference the published version.

## Take down policy

While the University of Birmingham exercises care and attention in making items available there are rare occasions when an item has been uploaded in error or has been deemed to be commercially or otherwise sensitive.

If you believe that this is the case for this document, please contact [UBIRA@lists.bham.ac.uk](mailto:UBIRA@lists.bham.ac.uk) providing details and we will remove access to the work immediately and investigate.

# Journal Pre-proof

Conformational states control Lck switching between free and confined diffusion modes in T cells

Geva Hilzenrat, Elvis Pandžić, Zhengmin Yang, Daniel J. Nieves, Jesse Goyette, Jérémie Rossy, Y. Ma, Katharina Gaus

PII: S0006-3495(20)30116-8

DOI: <https://doi.org/10.1016/j.bpj.2020.01.041>

Reference: BPJ 10296

To appear in: *Biophysical Journal*

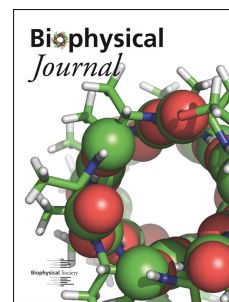
Received Date: 5 July 2019

Accepted Date: 23 January 2020

Please cite this article as: Hilzenrat G, Pandžić E, Yang Z, Nieves DJ, Goyette J, Rossy J, Ma Y, Gaus K, Conformational states control Lck switching between free and confined diffusion modes in T cells, *Biophysical Journal* (2020), doi: <https://doi.org/10.1016/j.bpj.2020.01.041>.

This is a PDF file of an article that has undergone enhancements after acceptance, such as the addition of a cover page and metadata, and formatting for readability, but it is not yet the definitive version of record. This version will undergo additional copyediting, typesetting and review before it is published in its final form, but we are providing this version to give early visibility of the article. Please note that, during the production process, errors may be discovered which could affect the content, and all legal disclaimers that apply to the journal pertain.

© 2020 Biophysical Society.



# Conformational states control Lck switching between free and confined diffusion modes in T cells

Geva Hilzenrat<sup>1, 2, 3</sup>, Elvis Pandžić<sup>4</sup>, Zhengmin Yang<sup>1, 2</sup>, Daniel J. Nieves<sup>1, 2, 5</sup>, Jesse Goyette<sup>1, 2</sup>, Jérémie Rossy<sup>6</sup>, Y. Ma<sup>1, 2</sup>, Katharina Gaus<sup>1, 2\*</sup>

<sup>1</sup>EMBL Australia Node in Single Molecule Science, School of Medical Sciences, University of New South Wales, Sydney, Australia

<sup>2</sup>ARC Centre of Excellence in Advanced Molecular Imaging, University of New South Wales, Sydney, Australia

<sup>3</sup>Commonwealth Scientific and Industry Research Organization (CSIRO), Manufacturing, Clayton, Victoria, Australia

<sup>4</sup>BioMedical Imaging Facility, Mark Wainwright Analytical Centre, University of New South Wales, Sydney, Australia

<sup>5</sup>Institute of Immunology and Immunotherapy, College of Medical and Dental Sciences, University of Birmingham, Birmingham, B15 2TT, UK.

<sup>6</sup>Biotechnology Institute Thurgau, University of Konstanz, Kreuzlingen, Switzerland

\*Corresponding author: k.gaus@unsw.edu.au

## Abstract

T cell receptor (TCR) phosphorylation by Lck is an essential step in T cell activation. It is known that the conformational states of Lck control enzymatic activity; however, the underlying principles of how Lck finds its substrate over the plasma membrane remain elusive. Here, single-particle tracking is paired with photoactivatable localization microscopy (sptPALM) to observe the diffusive modes of Lck in the plasma membrane. Individual Lck molecules switched between free and confined diffusion in both resting and stimulated T cells. Lck mutants locked in the open conformation were more confined than Lck mutants in the closed conformation. Further confinement of kinase-dead versions of Lck suggests that Lck confinement was not caused by phosphorylated substrates. Our data supports a model where confined diffusion of open Lck results in high local phosphorylation rates, and inactive, closed, Lck diffuses freely to enable long-range distribution over the plasma membrane.

## Statement of Significance

Phosphorylation of the TCR-CD3 complex by the kinase Lck is an essential step in T cell activation, but how membrane-bound Lck finds and phosphorylates its substrates is not well understood. Here, we examined the diffusive behavior of individual Lck molecules by single particle tracking in conjunction with photoactivatable localization microscopy (sptPALM). Our data demonstrate that Lck molecules frequently switch between confined and free diffusion and spent a prolonged time in the confined diffusion mode in stimulated T cells when the kinase is in the open conformation. This may underpin a dual-state search strategy in which open Lck exhibits confined diffusion, resulting in high local phosphorylation rates, and closed Lck diffuses freely to enable wide-range scanning of the plasma membrane.

## Introduction

T cell signaling is a tightly controlled process of simultaneous and sequential spatiotemporal events, involving membrane remodeling, and the redistribution of signaling proteins (1). Engagement of the T cell receptor (TCR) with an antigenic pMHC on the surface of an antigen-presenting cell (APC) leads to the formation of immunological synapses (2) and initiates downstream signaling events that lead to T cell activation (3). The Src family kinase Lck plays a crucial role in the signaling cascade. TCR engagement results in the membrane release (4) and phosphorylation of the immunoreceptor tyrosine-based motifs (ITAMs) located in the cytoplasmic tails of the CD3 $\zeta$  chain by Lck (5). Phosphorylated sites on the TCR-CD3 complex become docking sites for the zeta chain-associated protein kinase 70 (ZAP70), that is further phosphorylated by Lck (6) before recruiting other proteins in the signaling cascade that are necessary for complete T cell activation.

The kinase Lck, an essential TCR signaling protein, is a 56 kDa protein comprised of a Src homology (SH) 4 domain at the N-terminus, followed by a unique domain, an SH3 domain, an SH2 domain, a kinase domain, and a short C-terminal tail. Lck is anchored to the plasma membrane through its SH4 domain via post-translational acylation on three specific sites: a myristoylated Gly2 (7), and palmitoylated Cys3 and Cys5. The latter two enable membrane binding, and thus Lck diffusion in the inner leaflet of the plasma membrane (8). Notably, Lck is also found in the cytoplasm, as the palmitoylation is reversible (9), and is recruited to the immunological synapse. The unique domain interacts with the CD3 $\epsilon$  subunit in the TCR-CD3 complex (10), as well as the co-receptors CD4 and CD8 (11), via zinc-mediated bonds. However, Lck does not require the co-receptors for recruitment to the immunological synapse, or for TCR triggering (12), suggesting that freely diffusing Lck is sufficient for T cell activation.

Lck conformation is regulated by the phosphorylation of two tyrosine residues: Tyr<sup>394</sup>, whose phosphorylation increases Lck activity, and Tyr<sup>505</sup>, whose phosphorylation reduces Lck activity (13, 14). Intramolecular interactions between the phosphorylated Tyr<sup>505</sup> (pTyr<sup>505</sup>) and the SH3 and SH2 domains cause rearrangements that keep Lck in an inactive state (15, 16). When dephosphorylated by CD45, Lck exists in an open, primed conformation. When Tyr<sup>394</sup> is trans-autophosphorylated (14), rearrangements in the activation loop stabilize the active

conformation (17). The diffusion behavior (18) and conformational state of Lck (19, 20) are thought to be regulated by the activation state of the cell. The conformational state also influences Lck clustering (21). This means that not only does Lck conformational state regulate Lck enzymatic activity, but also aids in its diffusive search strategy.

Whether Lck becomes ‘active’, i.e., converted into the open conformation upon TCR engagement, has been controversial. There is evidence of global changes in relative populations of closed and open Lck in resting *versus* stimulated T cells (19, 20). These studies propose that Lck undergoes conformational changes upon T cell activation, driving it from its closed state to an open state, therefore enhancing its activity. Using biochemical analyses, conformational heterogeneity was observed in resting and stimulated T cells (22), suggesting a “standby-model” in which ~40% of Lck is in the open conformation in both resting and stimulated T cells. Ballek *et al.* challenged these observations in a later report that used different cell lysis conditions (23). Other studies, based on measurements of fluorescence resonance energy transfer (FRET) between fluorescent proteins fused to the N- and C-terminals of Lck, found that 62% of Lck was pre-activated in T cells (24), and concluded there was no significant change in open *versus* closed populations of Lck even after T cell stimulation (25). While different papers report different percentages of open Lck in pre-stimulated cells, constitutively active Lck was also found in CD8<sup>+</sup> memory T cells, and may account for the enhanced sensitivity to antigen in these cells (26). A pool of active Lck existing prior to T cell stimulation led to the idea that rapid TCR triggering post receptor engagement may be caused by changes in Lck spatial rearrangements as opposed to, or in addition to conformational changes. Using single-molecule localization microscopy in fixed cells, we previously showed that Lck distributed differently on the cell surface depending on its conformational state (21), with open Lck residing preferentially in clusters, and inactive Lck preventing clustering. However, this study only captured the overall distribution of open or inactive Lck, and the movement of Lck clusters, but to understand the search strategy of the membrane-bound kinase, the dynamic behavior of individual molecules needs to be taken into account.

The dynamic behavior of Lck was previously mapped with single particle tracking (SPT) in live cells, revealing, for example, the differences in Lck diffusion in stimulated *versus* resting T cells and the formation of microclusters, but without linking dynamics to conformational states (18, 27). Overall changes in diffusion constants were observed, as well as segregation into different confinement zones, attributed to actin and other proteins compartmentalizing the membrane (27, 28), or to the formation of membrane microdomains (18). Recently, Lck compartmentalization upon TCR stimulation was attributed to the formation of close-contact zones between the T cell membrane and the stimulating surface, possibly because of exclusion of CD45, in line with the kinetic segregation model (29). These works, however, did not take into account the conformational change in Lck.

In the current study, we utilize SPT using photoactivatable localization microscopy (sptPALM) (30) as a tool to study the diffusion of wild type (WT) and mutated Lck, lacking the tyrosine residues on positions 394 and 505, to measure the dynamics of the inactive and open forms, respectively (19, 20). Lck variants were tagged with photoactivatable monomeric

cherry (PAmCherry) (31), expressed in Jurkats E6.1 cells and imaged in resting and activating conditions. Single trajectories were extracted and analyzed in order to find periods when the proteins underwent confined diffusion, and the fraction of confined versus free proteins was determined (32). Measurements of different Lck variants showed that the open form of Lck spent more in confinements compared to the inactive form. Taken together, the data suggest that Lck continuously switched between open and closed states, a process that is likely to determine the probability of productive encounters between Lck and its substrates.

## Methods and Materials

### Plasmids

Lck and Lck10 were amplified by PCR and inserted within the *Ecot*1 and *Age*1 restriction sites of a pPAmCherry-N1 plasmid. Y394F, Y505F and K273R mutations were further introduced via site-directed mutagenesis.

### Sample Preparation

Jurkat cells were cultured in RPMI medium (Gibco) containing phenol-red and supplemented with 10% (vol/vol) FBS, 2 mM L-glutamine (Invitrogen), 1 mM penicillin (Invitrogen) and 1 mM streptomycin (Invitrogen). Cell cultures were passaged normally every ~48 hours, when the cell count reached  $\sim 8 \times 10^5$  viable cells per ml. The cells were cultured for at least 1 week (3-4 passages) after thawing prior to transfection and imaging. No cells were used after passage 20.

Cells were transfected by electroporation (Neon; Invitrogen); briefly, cells were collected before reaching a cell density of  $8 \times 10^5$  cell/ml and while  $\geq 90\%$  viable. The cells were washed twice with 1x PBS in 37°C and resuspended in the resuspension buffer (R-buffer) provided with the Neon kit. Three pulses of 1325 V with 10 ms duration were applied. The cells were allowed to recover in clear RPMI 1640 medium (Gibco) supplemented with 20% HI-FBS for overnight. Prior to imaging, fresh warm (37°C) media with 40 mM HEPES, pH 7.4 was added to achieve a final concentration of 20 mM HEPES.

1.5H coverslips (Marienfeld-Superior) were water bath-sonicated in four 30-minutes stages: 1 M KOH, Acetone, EtOH and ultra-pure (18 M $\Omega$ .cm) water. The coverslips were then allowed to adsorb 0.01% PLL (Sigma) in ultra-pure water for 15 minutes. Excess solution was later aspirated and the coverslips were baked-dry in 60 °C for 1 hour. Finally, after cooling-down, the coverslips were coated with either 0.01 mg/ml anti-CD3 (OKT3; eBioscience) and 0.01 mg/ml anti-CD28 (CD28.2; Invitrogen) for stimulating conditions or 0.01 mg/ml  $\alpha$ CD90 for (Thy-1; eBioscience) for resting conditions and let rest in 4°C overnight before imaging. The coverslips were washed 3 times with phosphate buffer saline (PBS) pre-warmed to 37°C before the cells were transferred onto them to interact with the antibodies. For live-cell experiments, imaging took place ~5 minutes after cell-transfer or fixed with 4%



paraformaldehyde (P6148; Sigma) in 37°C, followed by 3 washing cycles with PBS for fixed-cell imaging.

To verify the activation status of T cells, Jurkat E6.1 cells on resting and stimulating surfaces were fixed with 4% paraformaldehyde and immunostained with a primary antibody against CD3 $\zeta$  Y142 conjugated to Alexa Fluor 647 (K25-407.69, BD Biosciences). Fluorescence intensity was determined with TIRF microscopy (Zeiss Elyra) and analyzed as previously described (33). For Ca<sup>2+</sup> imaging in T cells, cells were loaded with Fluo-4, washed, incubated on the indicated surface for 15 min or kept in solution and imaged with confocal microscopy (Zeiss LSM780). Note, Jurkat cells exhibit Ca<sup>2+</sup> basal fluxes. To measure CD69 expression, 10<sup>6</sup> Jurkat E6.1 cells were stained with anti-human CD69 Alexa Fluor488 (310916, BioLegend) at 4°C for 30 min, placed on resting or stimulating surfaces or kept in solution, and analysed with flow cytometry (BD bioscience FACSanto II and FlowJo software).

## Imaging

For each sptPALM experiment 10,000 frames were acquired in a ~50 frames per second (18 ms exposure time) rate on a total internal reflection fluorescence (TIRF) microscope (ELYRA P1, Zeiss) in 37°C using a 100 $\times$  oil immersion objective (N.A. = 1.46) and a 67.5° incident beam angle. The frame rate was chosen to match mean-square displacement of 160 nm for a diffusion of 2  $\mu\text{m}^2/\text{sec}$ , which is below the size of a point spread function and fits well with our experiments where diffusion coefficients were < 2  $\mu\text{m}^2/\text{sec}$ . PAmCherry fused to Lck variants were continuously photoactivated using a 405 nm laser radiation tuned to 0.5-5  $\mu\text{W}$  (interchangeable during acquisition to maintain a low density) and continuously excited with a 561 nm laser tuned to 2.5 mW. Point density was monitored by using ZEN (Zeiss) online-processing tool.

## Data Analysis

All accumulated data are comprised of three biologically independent experiments, i.e., each mutant was imaged in two or more cells (in one of the three repetitions, where a repetition relates to a different transfection) in each cell-activation state (stimulated or resting). We used Diatrack (34) for fitting the point spread functions (PSFs) to a Gaussian with a 1.75 pixel width (1 pixel  $\approx$  0.097 nm) and then to track the particles by setting the search radius to 10 pixels. The data was later analyzed by a custom MATLAB (Mathworks) adaptation of the trajectory analysis part of a previously published multi-target tracing (MTT) code (32). Immobile particles (i.e., particles that had trajectories with an end-to-end distance of less than two pixels) and trajectories shorter than 15 frames were excluded from analysis. Stages of confined and free diffusion were detected according to equation 1, with  $D_{\text{free}} = 2.15 \mu\text{m}^2/\text{sec}$  (Fig. S2b, bottom),  $W = 4$  and  $t_w$  was the sum of the exposure time and the CCD reading time (~19.7 ms). To detect time spent in confinement, each sequence was segmented to non-overlapping windows of 5 frames and in each block of 5 frames, the ratio of confined:total particles was calculated. Each value of one 5 frames-window is a count in the histogram. The level of confinement,  $L_{\text{Conf}}$ , was calculated according to:

$$(1) L_{Conf} = \frac{D_{free} \times W \times t_w}{var(r)}$$

where  $D_{free}$  is the diffusion coefficient of freely diffusing Lck in  $\mu m^2 sec^{-1}$ ,  $W$  is the window size in frames,  $t_w$  is the temporal length of the window in seconds and  $var(r)$  is the variance in  $\mu m^2$ , which was determined for each window. All data processing and statistical analyses were performed in MATLAB.

## Statistical Tests

To compare between two populations of confinement fractions, that do not normally distribute, we used the Mann-Whitney U test, while the Kruskal-Wellis test was used for multiple datasets followed by a bonferroni post-hoc test. \*\*\*\* and n.s. indicate  $p \leq 0.00001$  and  $p > 0.01$ , respectively. Ranges around median and mean values in supplementary text are the 95% confidence intervals calculated from bootstrapping the data by sampling 10,000 times.

## Results and Discussion

The goal of this study was to determine whether the diffusion properties of individual Lck molecules were influenced by the conformational states of the kinase. Since Lck is found both in a cytosolic pool and attached to the inner leaflet of the plasma membrane (9), we chose sptPALM, since single molecule trajectories under TIRF illumination enable the quantification of only membrane bound Lck. To compare Lck in different conformational states requires the expression of Lck mutants. Because these mutants also impact on Lck activity, and hence the T cell activation status, it was necessary to express Lck in wild-type Jurkat cells that also express endogenous Lck (35). This allowed us, for example, to compare the diffusion of kinase-dead Lck in resting and activated cells since endogenous Lck facilitates T cell activation in cells that also express kinase-dead Lck. Notably, sptPALM experiments do not require high levels of overexpression, so the total levels of Lck can be kept within or close to the physiological range. Finally, we needed to control the T cell activation status. We chose to do this by seeding T cells onto activating and non-activating antibody-coated surfaces. These conditions not only result in controlled T cell activation (33), but also enable the recording of long single molecule trajectories. To determine whether individual Lck molecules switch between diffusion modes and gain statistical certainty, it is necessary to record large numbers of trajectory of sufficiently long durations. Alternative activation protocols such as protein-decorated supported lipid bilayers, are not ideal for SPT experiments as cells move laterally, with different speeds on activating and non-activating bilayers, and severely limit both the number of trajectories per cell and the length of each trajectory that can be recorded. While antibody-coated surfaces result in well-controlled T cell activation statuses (Fig. S1) and enabled sptPALM experiment, it should be noted that TCR clustering and mobility is different in T cells on antibody-coated surfaces compared to T cells on laterally mobile supports, with both protocols resulting in mobile and immobile TCRs under both activating and non-activating conditions (33). In summary, Jurkat E6.1 were transfected with either wild-type Lck (wtLck) fused to PAmCherry (wtLck-PAmCherry) or Lck variants, such as a truncated construct of Lck containing only the first



ten amino acids that are responsible for Lck anchoring to the membrane (Lck10-PAmCherry). T cells were incubated for 5 minutes at 37°C on a coverslip coated with anti-CD3 and anti-CD28 antibodies (stimulated) or anti-CD90 (resting), and then imaged, either in live-cell conditions, or after chemical fixation.

### Identification of free and confined states of Lck in live T cells

For each SPT experiment, we acquired 10,000 frames with an 18 ms exposure for the duration of ~197 s under TIRF illumination. While imaging was done with continuously photo-activating and exciting the fluorophores, the rate of photo-activation, and thus density of emitting fluorophores, was kept deliberately low in order to ensure only individual Lck molecules were tracked. Because Lck could be cytosolic, or found in fast moving cytosolic vesicles, which can appear briefly in the TIRF zone, we removed trajectories shorter than 15 frames. Likewise, immobile particles (see Methods) were excluded from analysis to eliminate Lck in cytosolic vesicles that were docked at the plasma membrane.

To address whether individual Lck molecules could switch between different diffusion modes, we employed a previously described post-tracking analysis that can distinguish between confined and free diffusion in each trajectory (Fig. S2) (32). Briefly, every trajectory is first fragmented into overlapping windows. For each window, the normalized variance of the location of the particle is calculated as a measure of the level of confinement,  $L_{Conf}$ , according to:

$$(2) L_{Conf} = \frac{D_{free} \times W \times t_w}{var(r)}$$

where  $D_{free}$  is the diffusion coefficient of freely diffusing Lck in  $\mu m^2 sec^{-1}$ ,  $W$  is the window size in frames,  $t_w$  is the temporal length of the window in seconds and  $var(r)$  is the variance in  $\mu m^2$ . For the value of  $D_{free}$ , we could not choose the diffusion coefficient of full-length Lck due to the broad distribution in diffusion coefficients, and because the potential protein-protein interactions, even in resting cells, may mean that full-length Lck may not solely diffuse freely. Thus, we chose the diffusion coefficient of  $2 \mu m^2 sec^{-1}$  for Lck10-PAmCherry (in resting T cells) for all versions of Lck, as Lck10 is membrane anchored and does not interact with other proteins. The  $L_{Conf}$  values for wtLck-PAmCherry in stimulated T cells falls largely between the  $L_{Conf}$  values for Lck10-PAmCherry in resting cells and wtLck-PAmCherry in fixed cells (Fig. 1A). Assuming that Lck10-PAmCherry in resting cells diffuses essentially freely, and wtLck-PAmCherry in fixed cells is permanently immobile. The data is evidence that wtLck-PAmCherry in stimulated T cells either has a homogeneous diffusion of intermediate speed, has two or more pools of Lck with different diffusion coefficients, or that individual Lck molecules alter between a fast/free diffusion mode and a slow/confined diffusion mode.

To test which of the three scenarios apply to wtLck-PAmCherry, we defined a threshold for  $L_{Conf}$ . We followed the published procedure (32) of choosing the most common  $L_{Conf}$  value (dotted line in Fig. 1A) of the protein of interest as the threshold. Importantly, the  $L_{Conf}$  threshold is defined in the ensemble measurement (i.e., the  $L_{Conf}$  histogram, Fig. 1A) and then

applied to individual Lck trajectories (Fig. 1B). To distinguish between confined Lck molecules and Lck molecules that temporarily slowed down, we only regarded a molecule as confined (yellow areas in Fig. 1B-C) if it has an  $L_{\text{Conf}}$  value above the threshold for three or more consecutive windows. If Lck diffusion is homogenous with an intermediate diffusion coefficient, this criterium would not be fulfilled, and no confinement zones would be detected in individual trajectories. If two pools of Lck exist that have different diffusion modes, but Lck molecules do not switch between diffusion modes while being tracked, the entire length of the trajectory would either be contained within or excluded from the confinement zone, i.e., there would be two types of trajectories. If, and only if, a molecule switched diffusion mode would part of the trajectory lay within a confinement zone and part outside the confinement zone (Fig. 1B-C). The latter was observed for almost all mobile trajectories of wtLck-PAMCherry in stimulated T cells (Fig. 1B-E), providing strong evidence that individual wtLck-PAMCherry molecules in live cells on activating antibody-coated surfaces switched between free and confined diffusive states (Fig. 1D-E). In contrast, in fixed cells, only confined or immobile molecules were observed (Fig. 1D-E).

### **Wild-type Lck was more confined in stimulated than resting T cells**

Our data strongly suggest that individual Lck molecules frequently switched between at least two diffusion modes, a more confined diffusion mode and a free diffusion mode. Since previous studies provided evidence that T cell activation decreases the overall diffusion of Lck (18, 27), we asked whether T cell activation altered the Lck diffusion mode overall, or altered the time spend in either diffusion mode. In our experiments, resting T cell data was generated by placing T cells expressing wtLck-PAMCherry onto coverslips coated with anti-CD90 antibodies. This resulted in good T cell adhesion (Fig. 2A), but not TCR signaling or T cell activation (Fig. S1) (33). On antibody-coated surfaces, T cell shape and contact size is broadly comparable for resting and stimulating conditions, with T cells often spreading more on the activating surface, but with considerable cell-cell variability under both conditions. Importantly, good cell adhesion meant that a high number of trajectories could be recorded under both cell conditions (Table 1). To visually compare the two conditions, we color-coded each trajectory according to their initial diffusion coefficient (Fig. 1A left with color code below) and applied the  $L_{\text{Conf}}$  threshold value to each trajectory (Fig. 1B right, same color code as Fig. 1). It can be seen that Lck overall diffused faster in resting cells with diffusion coefficients of  $1.16 \mu\text{m}^2 \text{s}^{-1}$  (1.15-1.17) to  $0.69 \mu\text{m}^2 \text{s}^{-1}$  (0.68-0.7) for resting and stimulated cells, respectively (Fig. 2A, Fig. S3a; Movie S1: resting - right, stimulated - left). Further, fewer confinement zones were detected for wtLck-PAMCherry in resting than stimulated cells (Fig. 1A). When comparing the  $L_{\text{Conf}}$  histogram of wtLck in stimulated T cells (Fig. 2B, blue) *versus* resting T cells (Fig. 2B, orange), it is noticeable that the values in activated cells are shifted to higher values, resulting in a mean  $L_{\text{Conf}}$  value of 32.9 in stimulated cells and 29.1 in resting cells.

Next, we examined whether the decrease in local displacement variance is due to a redistribution of wtLck-PAMCherry into confinements that would result in an increase in the number of consecutive steps that fall above the  $L_{\text{Conf}}$  threshold value. Thus, we segmented the total video into segments of five frames (Fig. S4), in which we asked how many particles, out

of the total number of particles imaged, were confined. Histograms obtained for stimulated and non-stimulated cells (Fig. 2C) were collected. There was a clear difference in the peak value for the two populations, as well as a larger tail of high values for wtLck-PAmCherry in stimulated cells. As a consequence, the populations were statistically different (Fig. 2C) when tested against the null hypothesis according to which the samples are drawn from the same population, using the rank sum test, with different medians and non-overlapping 95% confidence intervals with the values of 27.27% (26.67-27.78) and 22.22% (21.82-22.73) for stimulated and resting cells, respectively. The percentage of confined wtLck-PAmCherry were 31.0% (30.6-31.3) and 26.4% (26.1-26.7) in stimulated and resting cells, respectively.

Overall, these results show that wtLck-PAmCherry diffused slower in stimulated cells compared to resting cells because individual Lck molecules spent more time in confinement zones. These results are in agreement with an increase in wtLck-PAmCherry clustering in fixed stimulated *versus* fixed resting T cells (21). Confinement of Lck could be caused by lipid rafts (36, 37), microdomains (38, 39) and/or because Lck became trapped in protein clusters (18), such as TCR clusters (40). In our experiments, potential Lck binding partners were not fluorescent, and the low laser intensity made it unlikely that neighboring Lck molecules were photo-converted in the same imaging frame. Thus, it is not possible to classify detected Lck molecules as belonging to a Lck cluster, bound to the TCR, or other signaling proteins. Because we also observed that individual Lck molecules experience confinement in resting T cells, it is unlikely that all confinement events were caused by TCR signaling clusters since the TCR phosphorylation levels in resting T cells on antibody-coated surfaces was hardly detectable (Fig. S1). It should be noted that we previously found that Lck clusters in stimulated cells on antibody-coated surfaces were constantly remodeled, and not positionally stable (21), but it is possible that Lck confinement is caused by Lck clustering in stimulated T cells.

### **Membrane anchoring alone is not contributing to Lck confinement**

Lck confinement may be attributed to the formation of membrane domains, i.e., changes in membrane order, as a result of TCR triggering (41). We used a truncated version of Lck, Lck10, that contained the first ten amino acids that Lck anchors to the membrane via post-translational lipid modifications. If membrane domains are responsible for the slowdown and confinement of full-length Lck, Lck10 should also exhibit different diffusion in resting and activated T cells. Thus, we repeated the sptPALM experiments with Lck, again plotting the initial diffusion coefficient and confinement analysis for individual Lck 10 trajectories (Fig. 3A). Particularly when compared to full-length Lck (Fig. 2A), there was noticeably less difference in Lck10 diffusion in resting and stimulated T cells (Fig. 3A; Movie S2), although the latter appeared fully spread and activated. Indeed, the diffusion coefficients for Lck10-PAmCherry were very high, and similar in stimulating and resting conditions (Fig. S3b and Table 1). The overall level of confinement of Lck10-PAmCherry was almost identical for both resting and stimulated cells, with a peak  $L_{\text{Conf}}$  value of 7.2 and 7.7, respectively (Fig. 3B). These values were significantly different from the ones found for wtLck-PAmCherry, with most of the probability function having a value below the threshold. A histogram of confinement events (Fig. 3C) shows comparable peak values for both stimulated and resting

cells. No statistically significant difference was found between the two samples (Fig. 3C, top panel), as shown by median of 9.62% (9.43-9.8) and 9.68% (9.52-10.00) for Lck10-PAmCherry expressed in stimulated and resting cells, respectively. Further, the mean fraction of confined particles was also similar in stimulating and resting cells, with values of 14.0% (13.7-14.2) and 14.7% (14.5-15.0), respectively. These values were lower than those found for wtLck-PAmCherry, suggesting Lck10-PAmCherry was far less confined than wtLck-PAmCherry, even in stimulated cells. Our data is in agreement with previous work by Kusumi and colleagues that also showed different diffusions between a full-length Lck and Lck10 (27). Taken together, the data strongly suggest that the increased confinement observed for full-length wtLck-PAmCherry was not due to global changes in membrane organization or membrane domains (18), as confinement of Lck10 in resting and stimulated T cells was similar.

### **Open Lck is highly confined in stimulated and resting cells**

Next, we quantified the influence of conformation on confinement of Lck in live cells. First, we introduced a Tyrosine-to-Phenylalanine mutation at position 505 in Lck (Lck<sup>Y505F</sup>). The mutation prevents the binding of Lck pTyr<sup>505</sup> to its own SH2 domain. This mutation is well known as ‘constitutively open’ (19-21, 25, 42) and ‘hyperactive’ (13). It should be noted overexpression of Lck<sup>Y505F</sup> can lead to spontaneous, antigen-independent triggering of the TCR. To keep our experiments consistent throughout this study, we thus expressed Lck<sup>Y505F</sup>-PAmCherry to a similar level as wtLck-PAmCherry in Jurkat cells. The same sptPALM analysis as above yielded images pseudo-colored for initial diffusion and confinement (Fig. 4A; Movie S3). Resting cells still had a smaller surface contact zone than stimulated T cells despite the over-expression of Lck<sup>Y505F</sup>-PAmCherry.

An overall change in the diffusion constants due to cell activation was observed, with values of 0.65  $\mu\text{m}^2 \text{s}^{-1}$  (0.64-0.66) and 0.95  $\mu\text{m}^2 \text{s}^{-1}$  (0.94-0.96) in stimulated and resting cells, respectively (Fig. S3c and Table 1). Further,  $L_{\text{Conf}}$  values for Lck<sup>Y505F</sup>-PAmCherry were higher than that of wtLck-PAmCherry (Fig. 4B), with peak values of 39.28 and 42.53 in stimulated and resting cells, respectively, with < 50% of  $\log_{10}(L_{\text{Conf}})$  events above the confinement threshold. In contrast to wtLck-PAmCherry, the  $L_{\text{Conf}}$  distributions of Lck<sup>Y505F</sup>-PAmCherry were similar in resting and stimulated T cells despite the shoulder at low  $L_{\text{Conf}}$  values in resting cells. In both resting and activated T cells, Lck<sup>Y505F</sup>-PAmCherry was more confined than wtLck-PAmCherry. This was also observed in the histograms of the confined fractions (Fig. 4C), with a large population of Lck<sup>Y505F</sup> molecules falling into the right tail of the distribution. Importantly, unlike in the corresponding data for wtLck-PAmCherry, these values were not significantly different from each other (Fig. 4C, top), with median values and overlapping 95% confidence interval of 26.55% (26.32-26.67) and 26.39% (26.14-26.67) for stimulated and resting cells, respectively. The fractions of confined Lck<sup>Y505F</sup>-PAmCherry were 29.9% (29.6-30.11) and 30.0% (29.7-30.2) in stimulated and resting cells, respectively.

These data show that when Lck is locked in the open state, it is also driven into a more confined diffusive behavior, which is comparable with wtLck-PAmCherry in stimulated cells (Fig. S5). Given that Lck in the open conformation exhibited confined diffusion and

hyperactivity (13, 14), it is highly likely that the confined diffusion state results in high local phosphorylation rates. Open Lck may become preferentially trapped in protein clusters that form upon TCR triggering (18, 40), resulting in slower overall diffusion, and more confinement. However, open Lck was also strongly confined in resting T cells suggesting that protein clusters *per se* are not necessary to confine Lck. Confinement may be caused by enhanced protein-protein interactions including Lck self-association (21). If the level of confinement is indicative of the fraction of Lck in the open conformation, our data support the notion that TCR triggering results in a higher proportion of wild-type Lck in the open conformation (19, 20).

#### Inactive Lck is as confined as wild-type Lck in resting cells

To further investigate the hypothesis that Lck conformation regulates Lck diffusive behavior, we expressed an inactive form of Lck in Jurkat cells. A mutation in position 394 converting a tyrosine into phenylalanine (Lck<sup>Y394F</sup>) prevents its trans-autophosphorylation that is necessary for Lck activity and results in reduced-activity (14) or an inactive Lck (13), likely because of the hyper-phosphorylated Tyr505 that constitutively closes the enzyme (19). Despite the over-expression of Lck<sup>Y394F</sup>-PAmCherry, T cells adhered well on non-activating surfaces. Visual examination of Lck<sup>Y394F</sup>-PAmCherry suggests that closed Lck was rarely confined even in T cells on stimulating surfaces (Fig. 5A; Movie S4).

As with the wtLck and Lck<sup>Y505F</sup>, Lck<sup>Y394F</sup>-PAmCherry did undergo a decrease in diffusion coefficient due to stimulation, from  $1.24 \mu\text{m}^2 \text{s}^{-1}$  (1.22-1.26) in resting cells to  $0.88 \mu\text{m}^2 \text{s}^{-1}$  (0.87-0.89) in stimulated cells (Table 1, Fig. S3d). We applied the same sptPALM analysis to Lck<sup>Y394F</sup>-PAmCherry, and lower  $L_{\text{Conf}}$  values were obtained with peak values of 32.93 and 30.36 in stimulated and resting cells, respectively (Fig. 5B). Histograms of the fraction of confined Lck<sup>Y394F</sup>-PAmCherry showed the populations were skewed towards lower values, and also contained the shoulder at low  $L_{\text{Conf}}$  values (Fig. 5C). Similar to Lck<sup>Y505F</sup>-PAmCherry, Lck<sup>Y394F</sup>-PAmCherry showed no statistically significant difference between stimulated and resting cells (Fig. 5C, top panel), and medians of 22.22% (21.88-22.58) and 21.95% (21.43-22.22) for Lck<sup>Y394F</sup>-PAmCherry in stimulated and resting cells, respectively. The mean confinement fractions were 26.1% (25.9-26.3) and 26.2% (25.9-26.6) for Lck<sup>Y394F</sup>-PAmCherry in stimulated and resting cells, respectively. It is possible that the K273R mutation in Lck prevents the rearrangements in the activation loop that prevent interaction with other proteins, thus, limiting confinement (13). Our data are consistent with Wan *et al.* who also report a slower diffusion rate for Lck<sup>Y394F</sup> than wild-type Lck due to less Lck-Lck interactions (24).

The confinement fraction values we found for the inactive Lck were smaller than the ones found for the open Lck (Fig. S5), suggesting that each Lck activity or conformational state regulates Lck diffusion. Indeed, inactive Lck had a similar level of confinement as wtLck in resting cells while open Lck was similarly confined as wtLck in activated cells (Fig. S5). Thus, the data supports the notion that confinements are regulated by the conformational state of Lck with open Lck being more confined than inactive Lck.



## Lck conformation and activity determine confinement

To delineate Lck activity from Lck conformational state, we expressed a constitutively inactive Lck variant in which the lysine in position 273 in the kinase domain is replaced with Arginine (Lck<sup>K273R</sup>-PAmCherry, Fig. 6, Fig. S6), which has been shown to render Lck kinase-dead (43). Images of resting and activated T cells expressing Lck<sup>K273R</sup>-PAmCherry (Fig. 6A) and the  $L_{\text{Conf}}$  histogram (Fig. 6B) looked similar to images of T cells expressing wild-type Lck only, with the histogram again containing the shoulder at low  $L_{\text{Conf}}$  values. Different diffusion coefficients of  $0.82 \mu\text{m}^2 \text{s}^{-1}$  (0.81-0.83) and  $1.13 \mu\text{m}^2 \text{s}^{-1}$  (1.12-1.15) were observed for Lck<sup>K273R</sup>-PAmCherry in stimulated and resting cells, respectively (Table 1, Fig. S3e). However, similar  $L_{\text{Conf}}$  histograms, with values of 34.80 for stimulated and 37.58 for resting cells, were obtained (Fig. 6B, blue and orange) with no significant difference observed in the fraction of time spent confined (Fig 6C, blue and orange). Lck<sup>K273R</sup>-PAmCherry spent 25.8% (25.6-26.1) and 25.6% (25.4-25.9) of time confined in stimulated and resting cells, respectively (Fig 6C). Thus, the level of confinement of kinase-dead Lck did not depend on the T cell activation status as it did for wild-type Lck (Fig. S6), suggesting that trans-autophosphorylation of wild-type Lck (13) contributes to confinement.

To further test this hypothesis, we expressed a constitutively open, kinase-dead mutant Lck<sup>K273R, Y505F</sup>-PAmCherry. The images (Fig. 6A) and the  $L_{\text{Conf}}$  histogram (Fig. 6B) were similar to Lck<sup>K273R</sup>-PAmCherry. Lck<sup>K273R, Y505F</sup>-PAmCherry had slower diffusion coefficients of  $0.41 \mu\text{m}^2 \text{s}^{-1}$  (0.41-0.42) and  $0.51 \mu\text{m}^2 \text{s}^{-1}$  (0.5-0.51) in stimulated and resting cells, respectively (Fig. 6A; Fig. S3f; Movie S5), values that were slower than those obtained for Lck<sup>K273R</sup>-PAmCherry (Fig. S3e, f). Further, Lck<sup>K273R, Y505F</sup>-PAmCherry had higher  $L_{\text{Conf}}$  values in stimulated cells (Fig. 6C, purple and yellow) compared to resting cells (44.78 and 35.09, respectively). When comparing total trajectories, Lck<sup>K273R, Y505F</sup>-PAmCherry in stimulated cells was more confined than in resting cells and more than Lck<sup>K273R</sup> in both cell activation statuses (Fig. S6). These data support the notion that open, but not necessarily enzymatically active Lck confined the kinase in distinct zones in the plasma membrane. Lck<sup>K273R, Y505F</sup>-PAmCherry was more confined in stimulated cells (27.0% (26.8-27.2)) than resting cells (23.3% (23.1-23.5)). Moreover, the lowered confinement for the K273R-Y505F mutant in resting cells compared to stimulated cells excludes the possibility of confinement due to increase in hydrodynamic radius of the enzyme (Fig. S6).

Finally, we compared the level of confinement of open and inactive Lck mutations (Fig. S5). It should be noted that these mutants were expressed in wild-type Jurkat cells and thus contained endogenous, untagged wild-type Lck. It is possible that wild-type Lck affected the diffusion of mutant Lck. Taken together, our data suggest that diffusion behavior could be regulated by the conformational state of the enzyme. Lck<sup>Y394F</sup>-PAmCherry i.e. inactive Lck was less confined than wtLck-PAmCherry in stimulated cells and Lck<sup>Y505F</sup>-PAmCherry i.e. open Lck in stimulated and resting cells. Further, Lck<sup>Y394F</sup>-PAmCherry demonstrated similar confinement to that of wtLck-PAmCherry in resting cells. The values obtained for the open mutant, both in stimulated and resting cells were closer to the value that we obtained for wtLck-PAmCherry in stimulating conditions. Taken together, our data support the notion that the open conformational state of Lck may result in Lck confinement. Thus, a model emerges



in which the enzyme switches between open and closed conformation, which may result in a dual-state search strategy where open and active Lck is confined and closed and inactive Lck diffuses freely (Fig. 7).

## Conclusions

Phosphorylation of the TCR-CD3 complex by the kinase Lck is an essential step in T cell activation (44). While the link between phosphorylation state and activity in Lck is reasonably well established (45), how membrane bound Lck finds and phosphorylates its substrates is not well understood. Here we provide evidence that individual Lck molecules frequently switched between confined and free diffusion in resting and stimulated T cells. A possible driver for the switch in diffusion modes could be the conformational states of Lck, as open Lck exhibited more confined diffusion, and inactive or closed Lck exhibited more free diffusion. As it has been shown that auto-inhibited Src cannot bind substrates (46), this is consistent with a dual-state search strategy that enables Lck to redistribute over large areas of the membrane in its closed state, and high local activity to efficiently phosphorylate TCR-CD3 complexes at numerous sites in the open state. Lck interactions with other proteins (47-50) and lipids (51) could also contribute to the temporary confinement of Lck. While the mechanism or mechanisms for Lck confinement remain unknown, Lck conformation may control the probability of interactions with binding partners to modulate T cell signaling activity, particularly if confined Lck is predominately in the open and enzymatically active state.

For technical reasons, we used coverslips coated with antibodies for our sptPALM experiments, and this format may have impacted on the mobility of the TCR-CD3 complex under activating conditions. We have previously conducted a detailed analysis of the dynamics of the TCR-CD3 complex in T cells, and compared TCR mobility in T cells on supported lipid bilayers and activating antibodies (as used here) (33). Surprisingly, we found no differences in the percentage of mobile to immobile TCR complexes and clusters, but subtle changes with respect to cluster remodeling during movement. In T cells on supported lipid bilayers, TCR clusters moving towards the cell center and are increased in molecular density, while TCR clusters moving away from the cell center exhibited a loss in molecular density (33). This correlation was not readily observed in T cells on antibody-coated surfaces. It is possible that the movement and remodeling of TCR-CD3 complexes in T cells on immobilized antibodies impacted on Lck diffusion and confinement. In T cells activated on support lipid bilayers, only short sptPALM trajectories could be recorded that could not be used for a quantitative analysis of the diffusion modes of single Lck molecules. New imaging technology, such as lattice light-sheet microscopy, may reveal insights in Lck behavior when a T cell is in contact with antigen-presenting cell.

Dual-state search strategies have previously been demonstrated in other systems (52). For Lck, this strategy could entail a confined state that corresponds to high Lck activity while probing the local environment for substrates and a diffusive state that enables the kinase to distribute quickly over the entire membrane. Such a dual-state search strategy may account for the high fidelity of Lck-mediated phosphorylation of the available TCR-CD3 complexes

while also retaining high signaling sensitivity when membrane-detached cytosolic tails of the CD3 complex are limited. The former would be mediated by the high enzymatic activity in Lck clusters while the high level of diffusion of Lck in the closed state would enable the latter. In conclusion, a dual-state search strategy facilitated by the behavior of individual Lck molecules may be a regulatory mechanism in T cell activation.

## Acknowledgments

K.G. acknowledges funding from the ARC Centre of Excellence in Advanced Molecular Imaging (CE140100011), Australian Research Council (LP140100967 and DP130100269) and National Health and Medical Research Council of Australia (1059278 and 1037320). G.H. acknowledges the supported by an Australian Government Research Training Program (RTP) Scholarship.

## Author Contributions

GH performed experiments, modified analysis, analyzed data, and wrote manuscript. EP established analysis and helped write the manuscript. ZY was responsible for the generation of Lck constructs. DJN and JG aided in writing and drafting of the manuscript. JR provided guidance with experiments. KG designed the project, interpreted the data and wrote the manuscript.

## Conflicts of interests

The authors declare no conflicts of interests.

**Supplementary Materials**

**Fig. S1** TCR phosphorylation, calcium fluxes and CD69 expression in resting and activated T cells.

**Fig. S2** Relationship between Lck diffusion coefficient and confinement

**Fig. S3** Diffusion coefficients histograms of wtLck, Lck10, LckY505F, LckY394F, LckK273R and LckK273R, Y505F in stimulated and resting Jurkat cells

**Fig. S4** Illustration of confinement ratio analysis

**Fig. S5** Comparison of confinement analysis result

**Fig. S6** Comparison of confinement analysis result of wtLck-PAmCherry, LckK273R-PAmCherry and LckK273R, Y505F-PAmCherry in stimulated and resting cells

**Movie S1**

**Movie S2**

**Movie S3**

**Movie S4**

**Movie S5**

558 **References**

- 559 1. Klammt, C., and B. F. Lillemeier. 2012. How membrane structures control T cell  
560 signaling. *Front Immunol* 3:291.
- 561 2. Dustin, M. L. 2014. The immunological synapse. *Cancer Immunol Res* 2(11):1023-1033.
- 562 3. Carreno, L. J., E. M. Riquelme, P. A. Gonzalez, N. Espagnol, C. A. Riedel, S. Valitutti, and  
563 A. M. Kalergis. 2010. T-cell antagonism by short half-life pMHC ligands can be mediated by  
564 an efficient trapping of T-cell polarization toward the APC. *Proc Natl Acad Sci U S A*  
565 107(1):210-215.
- 566 4. van der Merwe, P. A., H. Zhang, and S. P. Cordoba. 2012. Why do some T cell receptor  
567 cytoplasmic domains associate with the plasma membrane? *Front Immunol* 3:29.
- 568 5. Rossy, J., D. J. Williamson, and K. Gaus. 2012. How does the kinase Lck phosphorylate the T  
569 cell receptor? Spatial organization as a regulatory mechanism. *Front Immunol* 3:167.
- 570 6. Weiss, A. 1993. T cell antigen receptor signal transduction: a tale of tails and cytoplasmic  
571 protein-tyrosine kinases. *Cell* 73(2):209-212.
- 572 7. Kabouridis, P. S., A. I. Magee, and S. C. Ley. 1997. S-acylation of LCK protein tyrosine  
573 kinase is essential for its signalling function in T lymphocytes. *EMBO J* 16(16):4983-4998.
- 574 8. Yurchak, L. K., and B. M. Sefton. 1995. Palmitoylation of either Cys-3 or Cys-5 is required  
575 for the biological activity of the Lck tyrosine protein kinase. *Mol Cell Biol* 15(12):6914-6922.
- 576 9. Zimmermann, L., W. Paster, J. Weghuber, P. Eckerstorfer, H. Stockinger, and G. J. Schütz.  
577 2010. Direct Observation and Quantitative Analysis of Lck Exchange between Plasma  
578 Membrane and Cytosol in Living T Cells. *Journal of Biological Chemistry* 285(9):6063-6070.
- 579 10. Li, L., X. Guo, X. Shi, C. Li, W. Wu, C. Yan, H. Wang, H. Li, and C. Xu. 2017. Ionic CD3-  
580 Lck interaction regulates the initiation of T-cell receptor signaling. *Proc Natl Acad Sci U S A*  
581 114(29):E5891-E5899.
- 582 11. Briese, L., and D. Willbold. 2003. Structure determination of human Lck unique and SH3  
583 domains by nuclear magnetic resonance spectroscopy. *BMC Structural Biology* 3(1):3.  
584 journal article.
- 585 12. Casas, J., J. Brzostek, V. I. Zarnitsyna, J.-s. Hong, Q. Wei, J. A. H. Hoerter, G. Fu, J.  
586 Ampudia, R. Zamoyska, C. Zhu, and N. R. J. Gascoigne. 2014. Ligand-engaged TCR is  
587 triggered by Lck not associated with CD8 coreceptor. *Nature Communications* 5:5624.  
588 Article.
- 589 13. Liaunardy-Jopeace, A., B. L. Murton, M. Mahesh, J. W. Chin, and J. R. James. 2017.  
590 Encoding optical control in LCK kinase to quantitatively investigate its activity in live cells.  
591 *Nat Struct Mol Biol* 24(12):1155-1163.
- 592 14. Hui, E., and R. D. Vale. 2014. In vitro membrane reconstitution of the T-cell receptor  
593 proximal signaling network. *Nat Struct Mol Biol* 21(2):133-142.
- 594 15. Nika, K., L. Tautz, Y. Arimura, T. Vang, S. Williams, and T. Mustelin. 2007. A weak Lck tail  
595 bite is necessary for Lck function in T cell antigen receptor signaling. *J Biol Chem*  
596 282(49):36000-36009.
- 597 16. Gervais, F. G., L. M. Chow, J. M. Lee, P. E. Branton, and A. Veillette. 1993. The SH2  
598 domain is required for stable phosphorylation of p56lck at tyrosine 505, the negative  
599 regulatory site. *Mol Cell Biol* 13(11):7112-7121.
- 600 17. Davis, S. J., and P. A. van der Merwe. 2011. Lck and the nature of the T cell receptor trigger.  
601 *Trends in Immunology* 32(1):1-5.
- 602 18. Douglass, A. D., and R. D. Vale. 2005. Single-molecule microscopy reveals plasma  
603 membrane microdomains created by protein-protein networks that exclude or trap signaling  
604 molecules in T cells. *Cell* 121(6):937-950.
- 605 19. Philipsen, L., A. V. Reddycherla, R. Hartig, J. Gumz, M. Kastle, A. Kritikos, M. P. Poltorak,  
606 Y. Prokazov, E. Turbin, A. Weber, W. Zuschratter, B. Schraven, L. Simeoni, and A. J.  
607 Muller. 2017. De novo phosphorylation and conformational opening of the tyrosine kinase  
608 Lck act in concert to initiate T cell receptor signaling. *Sci Signal* 10(462).
- 609 20. Stirnweiss, A., R. Hartig, S. Gieseler, J. A. Lindquist, P. Reichardt, L. Philipsen, L. Simeoni,  
610 M. Poltorak, C. Merten, W. Zuschratter, Y. Prokazov, W. Paster, H. Stockinger, T. Harder,

- 611 M. Gunzer, and B. Schraven. 2013. T cell activation results in conformational changes in the  
612 Src family kinase Lck to induce its activation. *Sci Signal* 6(263):ra13.
- 613 21. Rossy, J., D. M. Owen, D. J. Williamson, Z. Yang, and K. Gaus. 2013. Conformational states  
614 of the kinase Lck regulate clustering in early T cell signaling. *Nat Immunol* 14(1):82-89.
- 615 22. Nika, K., C. Soldani, M. Salek, W. Paster, A. Gray, R. Etzensperger, L. Fugger, P. Polzella,  
616 V. Cerundolo, O. Dushek, T. Hofer, A. Viola, and O. Acuto. 2010. Constitutively active Lck  
617 kinase in T cells drives antigen receptor signal transduction. *Immunity* 32(6):766-777.
- 618 23. Ballek, O., J. Valecka, J. Manning, and D. Filipp. 2015. The pool of preactivated Lck in the  
619 initiation of T-cell signaling: a critical re-evaluation of the Lck standby model. *Immunol Cell*  
620 *Biol* 93(4):384-395.
- 621 24. Wan, R., J. Wu, M. Ouyang, L. Lei, J. Wei, Q. Peng, R. Harrison, Y. Wu, B. Cheng, K. Li, C.  
622 Zhu, L. Tang, Y. Wang, and S. Lu. 2019. Biophysical basis underlying dynamic Lck  
623 activation visualized by ZapLck FRET biosensor. *Science Advances* 5(6):eaau2001.
- 624 25. Paster, W., C. Paar, P. Eckerstorfer, A. Jakober, K. Drbal, G. J. Schutz, A. Sonnleitner, and H.  
625 Stockinger. 2009. Genetically encoded Forster resonance energy transfer sensors for the  
626 conformation of the Src family kinase Lck. *J Immunol* 182(4):2160-2167.
- 627 26. Moogk, D., S. Zhong, Z. Yu, I. Liadi, W. Rittase, V. Fang, J. Dougherty, A. Perez-Garcia, I.  
628 Osman, C. Zhu, N. Varadarajan, N. P. Restifo, A. B. Frey, and M. Krogsgaard. 2016.  
629 Constitutive Lck Activity Drives Sensitivity Differences between CD8+ Memory T Cell  
630 Subsets. *J Immunol* 197(2):644-654.
- 631 27. Ike, H., A. Kosugi, A. Kato, R. Iino, H. Hirano, T. Fujiwara, K. Ritchie, and A. Kusumi.  
632 2003. Mechanism of Lck recruitment to the T-cell receptor cluster as studied by single-  
633 molecule-fluorescence video imaging. *Chemphyschem* 4(6):620-626.
- 634 28. Ballek, O., J. Valecka, M. Dobesova, A. Brouckova, J. Manning, P. Rehulka, J. Stulik, and D.  
635 Filipp. 2016. TCR Triggering Induces the Formation of Lck-RACK1-Actinin-1 Multiprotein  
636 Network Affecting Lck Redistribution. *Front Immunol* 7:449.
- 637 29. Fernandes, R. A., K. A. Ganzinger, J. Tzou, P. Jonsson, S. F. Lee, M. Palayret, A. M. Santos,  
638 V. T. Chang, C. Macleod, B. C. Lagerholm, A. E. Lindsay, O. Dushek, A. Tilevik, S. J.  
639 Davis, and D. Klenerman. 2017. Constraining CD45 exclusion at close-contacts provides a  
640 mechanism for discriminatory T-cell receptor signalling. *bioRxiv*.
- 641 30. Manley, S., J. M. Gillette, G. H. Patterson, H. Shroff, H. F. Hess, E. Betzig, and J. Lippincott-  
642 Schwartz. 2008. High-density mapping of single-molecule trajectories with photoactivated  
643 localization microscopy. *Nat Methods* 5(2):155-157.
- 644 31. Subach, F. V., G. H. Patterson, S. Manley, J. M. Gillette, J. Lippincott-Schwartz, and V. V.  
645 Verkhusha. 2009. Photoactivatable mCherry for high-resolution two-color fluorescence  
646 microscopy. *Nat Methods* 6(2):153-159.
- 647 32. Serge, A., N. Bertaux, H. Rigneault, and D. Marguet. 2008. Dynamic multiple-target tracing  
648 to probe spatiotemporal cartography of cell membranes. *Nat Methods* 5(8):687-694.
- 649 33. Ma, Y., E. Pandzic, P. R. Nicovich, Y. Yamamoto, J. Kwiatek, S. V. Pagoon, A. Benda, J.  
650 Rossy, and K. Gaus. 2017. An intermolecular FRET sensor detects the dynamics of T cell  
651 receptor clustering. *Nat Commun* 8:15100.
- 652 34. Vallotton, P., and S. Olivier. 2013. Tri-track: free software for large-scale particle tracking.  
653 *Microsc Microanal* 19(2):451-460.
- 654 35. Straus, D. B., and A. Weiss. 1992. Genetic evidence for the involvement of the lck tyrosine  
655 kinase in signal transduction through the T cell antigen receptor. *Cell* 70(4):585-593.
- 656 36. Jordan, S., and W. Rodgers. 2003. T cell glycolipid-enriched membrane domains are  
657 constitutively assembled as membrane patches that translocate to immune synapses. *J*  
658 *Immunol* 171(1):78-87.
- 659 37. Ventimiglia, L. N., and M. A. Alonso. 2013. The role of membrane rafts in Lck transport,  
660 regulation and signalling in T-cells. *Biochem J* 454(2):169-179.
- 661 38. Ilangumaran, S., S. Arni, G. van Echten-Deckert, B. Borisch, and D. C. Hoessli. 1999.  
662 Microdomain-dependent regulation of Lck and Fyn protein-tyrosine kinases in T lymphocyte  
663 plasma membranes. *Mol Biol Cell* 10(4):891-905.
- 664 39. Filipp, D., O. Ballek, and J. Manning. 2012. Lck, Membrane Microdomains, and TCR  
665 Triggering Machinery: Defining the New Rules of Engagement. *Front Immunol* 3:155.

40. Pagoon, S. V., T. Tabarin, Y. Yamamoto, Y. Ma, P. R. Nicovich, J. S. Bridgeman, A. Cohnen, C. Benzing, Y. Gao, M. D. Crowther, K. Tungatt, G. Dolton, A. K. Sewell, D. A. Price, O. Acuto, R. G. Parton, J. J. Gooding, J. Rossy, J. Rossjohn, and K. Gaus. 2016. Functional role of T-cell receptor nanoclusters in signal initiation and antigen discrimination. *Proceedings of the National Academy of Sciences* 113(37):E5454-E5463.
41. Gaus, K., E. Chklovskaya, B. Fazekas de St Groth, W. Jessup, and T. Harder. 2005. Condensation of the plasma membrane at the site of T lymphocyte activation. *J Cell Biol* 171(1):121-131.
42. Ledbetter, J. A., J. P. Deans, A. Aruffo, L. S. Grosmaire, S. B. Kanner, J. B. Bolen, and G. L. Schieven. 1993. CD4, CD8 and the role of CD45 in T-cell activation. *Current Opinion in Immunology* 5(3):334-340.
43. Laham, L. E., N. Mukhopadhyay, and T. M. Roberts. 2000. The activation loop in Lck regulates oncogenic potential by inhibiting basal kinase activity and restricting substrate specificity. *Oncogene* 19(35):3961-3970.
44. Chakraborty, A. K., and A. Weiss. 2014. Insights into the initiation of TCR signaling. *Nat Immunol* 15(9):798-807.
45. D'Oro, U., K. Sakaguchi, E. Appella, and J. D. Ashwell. 1996. Mutational analysis of Lck in CD45-negative T cells: dominant role of tyrosine 394 phosphorylation in kinase activity. *Mol Cell Biol* 16(9):4996-5003.
46. Xu, W., A. Doshi, M. Lei, M. J. Eck, and S. C. Harrison. 1999. Crystal Structures of c-Src Reveal Features of Its Autoinhibitory Mechanism. *Molecular Cell* 3(5):629-638.
47. Courtney, A. H., J. F. Amacher, T. A. Kadlecsek, M. N. Mollenauer, B. B. Au-Yeung, J. Kuriyan, and A. Weiss. 2017. A Phosphosite within the SH2 Domain of Lck Regulates Its Activation by CD45. *Mol Cell* 67(3):498-511 e496.
48. Dobbins, J., E. Gagnon, J. Godec, J. Pyrdol, D. A. Vignali, A. H. Sharpe, and K. W. Wucherpfennig. 2016. Binding of the cytoplasmic domain of CD28 to the plasma membrane inhibits Lck recruitment and signaling. *Sci Signal* 9(438):ra75.
49. Filipp, D., B. Moemeni, A. Ferzoco, K. Kathirkamathamby, J. Zhang, O. Ballek, D. Davidson, A. Veillette, and M. Julius. 2008. Lck-dependent Fyn activation requires C terminus-dependent targeting of kinase-active Lck to lipid rafts. *J Biol Chem* 283(39):26409-26422.
50. Kapoor-Kaushik, N., E. Hinde, E. B. Compeer, Y. Yamamoto, F. Kraus, Z. Yang, J. Lou, S. V. Pagoon, T. Tabarin, K. Gaus, and J. Rossy. 2016. Distinct Mechanisms Regulate Lck Spatial Organization in Activated T Cells. *Front Immunol* 7:83.
51. Sheng, R., D. J. Jung, A. Silkov, H. Kim, I. Singaram, Z. G. Wang, Y. Xin, E. Kim, M. J. Park, P. Thiagarajan-Rosenkranz, S. Smrt, B. Honig, K. Baek, S. Ryu, J. Lorieu, Y. M. Kim, and W. Cho. 2016. Lipids Regulate Lck Protein Activity through Their Interactions with the Lck Src Homology 2 Domain. *J Biol Chem* 291(34):17639-17650.
52. Bénichou, O., C. Loverdo, M. Moreau, and R. Voituriez. 2011. Intermittent search strategies. *Reviews of Modern Physics* 83(1):81-129.



	Resting T cells	Stimulated T cells
wtLck-PAmCherry	D = $1.16 \mu\text{m}^2 \text{s}^{-1}$ (1.15-1.17) Confined: 26.4% (26.1-26.7) $N_{\text{total}} = 34,309$ $N_{\text{immobile}} = 2,929$ (8.54%)	D = $0.69 \mu\text{m}^2 \text{s}^{-1}$ (0.68-0.7) Confined: 31.0% (30.6-31.3) $N_{\text{total}} = 21,065$ $N_{\text{immobile}} = 2,508$ (11.91%)
Lck10-PAmCherry	D = $2.15 \mu\text{m}^2 \text{s}^{-1}$ (2.14-2.17) Confined: 14.7% (14.5-15.0) $N_{\text{total}} = 53,357$ $N_{\text{immobile}} = 805$ (1.51 %)	D = $2.08 \mu\text{m}^2 \text{s}^{-1}$ (2.07-2.09) Confined: 14.0% (13.7-14.2) $N_{\text{total}} = 67,352$ $N_{\text{immobile}} = 1,526$ (2.27 %)
Lck <sup>Y505F</sup> -PAmCherry	D = $0.95 \mu\text{m}^2 \text{s}^{-1}$ (0.94-0.96) Confined: 30.0% (29.7-30.2) $N_{\text{total}} = 41,127$ $N_{\text{immobile}} = 3,650$ (8.87%)	D = $0.65 \mu\text{m}^2 \text{s}^{-1}$ (0.64-0.66) Confined: 29.9% (29.6-30.11) $N_{\text{total}} = 32,024$ $N_{\text{immobile}} = 4,467$ (13.95%)
Lck <sup>Y394F</sup> -PAmCherry	D = $1.24 \mu\text{m}^2 \text{s}^{-1}$ (1.22-1.26) Confined: 26.2% (25.9-26.6) $N_{\text{total}} = 21,309$ $N_{\text{immobile}} = 1,350$ (6.34%)	D = $0.88 \mu\text{m}^2 \text{s}^{-1}$ (0.87-0.89) Confined: 26.1% (25.9-26.3) $N_{\text{total}} = 32,477$ $N_{\text{immobile}} = 2,921$ (8.99 %)
Lck <sup>K273R</sup> -PAmCherry	D = $1.13 \mu\text{m}^2 \text{s}^{-1}$ (1.12-1.15) Confined: 25.6% (25.4-25.9) $N_{\text{total}} = 31,025$ $N_{\text{immobile}} = 2,251$ (7.26 %)	D = $0.82 \mu\text{m}^2 \text{s}^{-1}$ (0.81-0.83) Confined: 25.8% (25.6-26.1) $N_{\text{total}} = 26,059$ $N_{\text{immobile}} = 2,479$ (9.51 %)
Lck <sup>K273R, Y505F</sup> -PAmCherry	D = $0.51 \mu\text{m}^2 \text{s}^{-1}$ (0.5-0.51) Confined: 23.3% (23.1-23.5) $N_{\text{total}} = 35,712$ $N_{\text{immobile}} = 4,945$ (13.85%)	D = $0.41 \mu\text{m}^2 \text{s}^{-1}$ (0.41-0.42) Confined: 27.0% (26.8-27.2) $N_{\text{total}} = 50,734$ $N_{\text{immobile}} = 9,168$ (18.07%)

707

708 **Table 1: Diffusion coefficients and confinement of wild-type Lck, Lck10 and Lck mutations**  
709 **obtained by single particle tracking.** Average diffusion coefficient, D, and percentage of  
710 confinement were extracted from the single particle analysis for Lck and Lck10 in Jurkat cells on  
711 resting and stimulating surfaces. 95% confidence values are listed in brackets.  $N_{\text{total}}$  refers to the total  
712 number of trajectories detected prior to analysis (including immobile trajectories) and  $N_{\text{immobile}}$  is the  
713 number of immobile particles that were excluded from the analysis. The percentage is  $N_{\text{immobile}}/N_{\text{total}}$ .

## 714 Figure Legends

715 **Fig. 1 Lck switches between free and confined states.** (A)  $L_{\text{Conf}}$  acquired for Lck10-  
 716 PAmCherry in resting Jurkat cells (purple), wtLck-PAmCherry in stimulated Jurkat cells  
 717 (orange) and wtLck-PAmCherry in fixed cells (cyan), normalized to peak value. The dashed  
 718 vertical line marks the threshold where a particle was to be considered confined, i.e., if it had  
 719 three or more consecutive steps with an  $L_{\text{Conf}}$  value greater than that threshold. (B) An  
 720 experimental trajectory decomposed to free (magenta) and confined (cyan) states, with the  
 721 confinements highlighted in yellow circles. (C) Time evolution of  $L_{\text{Conf}}$  values for the  
 722 trajectory in (B) with the threshold marked with an orange dashed line and the confined  
 723 periods with a yellow shade. (D) Trajectory decomposition maps of wtLck-PAmCherry in a  
 724 stimulated live cells (left) and fixed Jurkat cells (right) Free periods are colored magenta,  
 725 whereas confined periods are colored cyan. Scale bar = 5  $\mu\text{m}$ . (E) 5  $\mu\text{m}$  by 5  $\mu\text{m}$  zoomed-in  
 726 regions of interest in (D) (top – live, bottom - fixed). Scale bar = 1  $\mu\text{m}$ .

727 **Fig. 2 wtLck-PAmCherry is more confined in stimulated cells.** (A) Representative  
 728 stimulated and resting Jurkat E6-1 cells expressing wtLck-PAmCherry. The left panels show  
 729 bright field images of the cells with detected trajectories overlaid, color-coded according to  
 730 their initial diffusion. The right panels show the free (magenta) and confined (cyan) modes of  
 731 diffusion. Scale bar = 5  $\mu\text{m}$ . Bottom: diffusions histogram corresponding to the cells above,  
 732 sharing mutual color-coding. (B)  $L_{\text{Conf}}$  histograms for wtLck-PAmCherry in resting (orange)  
 733 and stimulated (blue) cells. (C) Histograms of the fraction of confined wtLck-PAmCherry  
 734 molecules obtained for 13 stimulated (blue) and 17 resting (orange) Jurkat cells. Box plot  
 735 shows the median. Notch 95% confidence interval, box edges first and third quartile, lines  
 736 Tukey's fences, \*\*\*\*  $p \leq 0.00001$ .

737 **Fig. 3 Lck10-PAmCherry demonstrates free-diffusion in resting and stimulated cells.**  
 738 (A) Representative stimulated and resting Jurkat E6-1 cells expressing Lck10-PAmCherry.  
 739 The left panels show bright field images of the cells with detected trajectories overlaid, color-  
 740 coded according to their initial diffusion. The right panels show the free (magenta) and  
 741 confined (cyan) modes of diffusion. Scale bar = 5  $\mu\text{m}$ . Bottom: diffusions histogram  
 742 corresponding to the cells above, sharing mutual color-coding. (B)  $L_{\text{Conf}}$  histograms for  
 743 Lck10-PAmCherry in resting (orange) and stimulated (blue) cells. (C) Histograms of the  
 744 fraction of confined Lck10-PAmCherry molecules obtained for 19 stimulated (blue) and 15  
 745 resting (orange) Jurkat cells. Box plot shows the median. Notch 95% confidence interval, box  
 746 edges first and third quartile, lines Tukey's fences, n.s.  $p > 0.01$ .

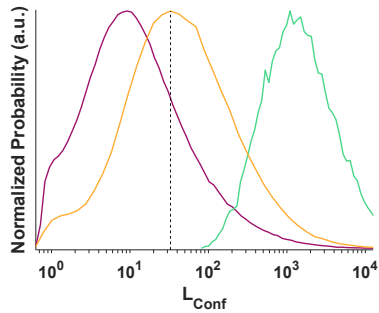
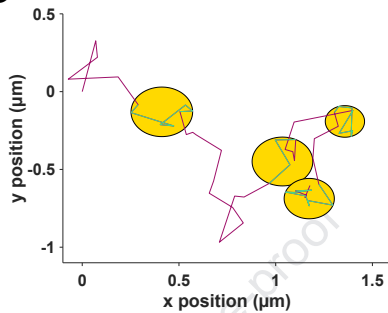
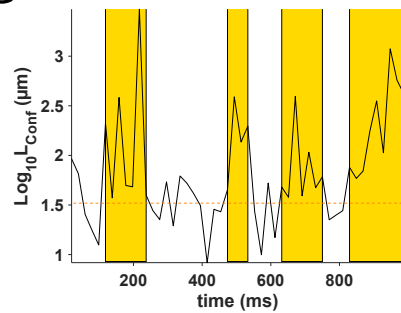
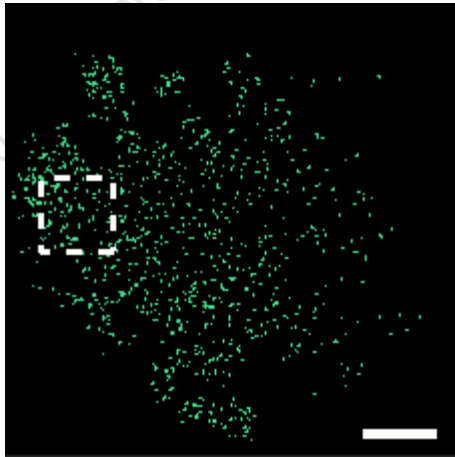
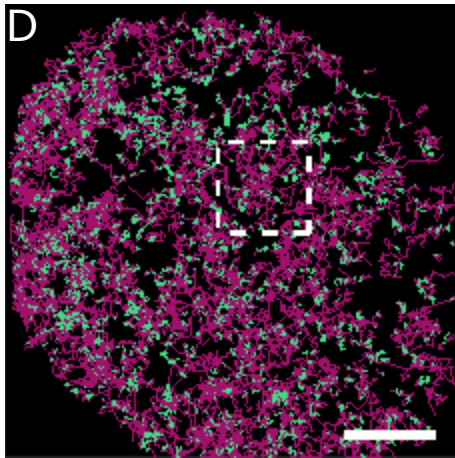
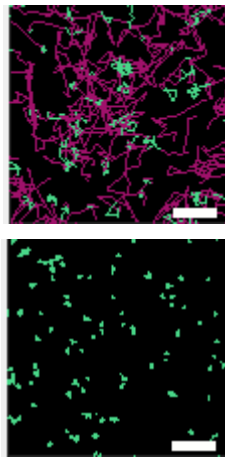
747 **Fig. 4 Lck<sup>Y505F</sup>-PAmCherry is equally confined in stimulated and resting cells.** (A)  
 748 Representative stimulated and resting Jurkat E6-1 cells expressing Lck<sup>Y505F</sup>-PAmCherry. The  
 749 left panels show bright field images of the cells with detected trajectories overlaid, color-  
 750 coded according to their initial diffusion. The right panels show the free (magenta) and  
 751 confined (cyan) modes of diffusion. Scale bar = 5  $\mu\text{m}$ . Bottom: diffusions histogram  
 752 corresponding to the cells above, sharing mutual color-coding. (B)  $L_{\text{Conf}}$  histograms for  
 753 Lck<sup>Y505F</sup>-PAmCherry in resting (orange) and stimulated (blue) cells. (C) Histograms of the  
 754 fraction of confined Lck<sup>Y505F</sup>-PAmCherry molecules obtained for 14 stimulated (blue) and 18

resting (orange) Jurkat cells. Box plot shows the median. Notch 95% confidence interval, box edges first and third quartile, lines Tukey's fences, n.s.  $p>0.01$ .

**Fig. 5 Lck<sup>Y394F</sup>-PAmCherry is equally confined in stimulated and resting cells.** (A) Representative stimulated and resting Jurkat E6-1 cells expressing Lck<sup>Y394F</sup>-PAmCherry. The left panels show bright field images of the cells with detected trajectories overlaid, color-coded according to their initial diffusion. The right panels show the free (magenta) and confined (cyan) modes of diffusion. Scale bar = 5  $\mu\text{m}$ . Bottom: diffusions histogram corresponding to the cells above, sharing mutual color-coding. (B)  $L_{\text{Conf}}$  histograms for Lck<sup>Y394F</sup>-PAmCherry in resting (orange) and stimulated (blue) cells. (C) Histograms of the fraction of confined Lck<sup>Y394F</sup>-PAmCherry molecules obtained for 16 stimulated (blue) and 14 resting (orange) Jurkat cells. Box plot shows the median. Notch 95% confidence interval, box edges first and third quartile, lines Tukey's fences, n.s.  $p>0.01$ .

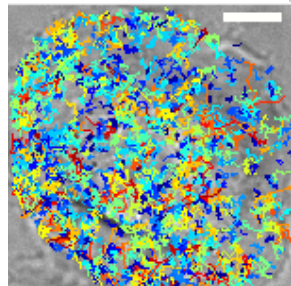
**Fig. 6 Confinement analyses for Lck<sup>K273R</sup>-PAmCherry and Lck<sup>K273R, Y505F</sup>-PAmCherry in stimulated and resting cells.** (A) Representative stimulated and resting Jurkat E6-1 cells expressing Lck<sup>K273R</sup>-PAmCherry and Lck<sup>K273R, Y505F</sup>-PAmCherry. The left panels show bright field images of the cells with detected trajectories overlaid, color-coded according to their initial diffusion. The right panels show the free (magenta) and confined (cyan) modes of diffusion. Scale bar = 5  $\mu\text{m}$ . Bottom: diffusions histogram corresponding to the cells above, sharing mutual color-coding. (B)  $L_{\text{Conf}}$  histograms for Lck<sup>K273R</sup>-PAmCherry and Lck<sup>K273R, Y505F</sup>-PAmCherry in and stimulated cells. (orange, blue, purple and yellow, respectively). (C) Histograms of the fraction of confined Lck<sup>K273R</sup>-PAmCherry molecules obtained for 12 stimulated (blue) and 14 resting (orange) Jurkat cells and histograms of the fraction of confined Lck<sup>K273R, Y505F</sup>-PAmCherry obtained for 8 stimulated (yellow) and 8 resting (purple) Jurkat cells. Box plot shows the median. Notch 95% confidence interval, box edges first and third quartile, lines Tukey's fences, , \*\*\*\*  $p\leq 0.00001$ , n.s.  $p>0.01$ .

**Fig. 7. Lck molecules switch between a confined and free diffusion modes.** Lck (illustrated in blue) exists in two main conformations: a closed conformation characterized by low catalytic activity and mediated by intramolecular interactions; and an open conformation characterized by high catalytic activity and free SH2 and SH3 domains. Our data propose that the closed conformation diffuses unimpeded (purple line), whereas the open conformation interacts with other membrane proteins (illustrated in green) via SH2 and SH3 domain mediated interactions and becomes confined (yellow circles) through rapid rebinding (teal line). This may result in a dual-stage search strategy where free diffusion allows Lck to relocate over large membrane areas while confinement in the open conformation enables high substrate phosphorylation rates.

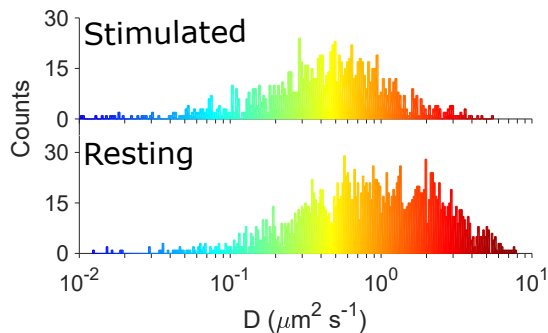
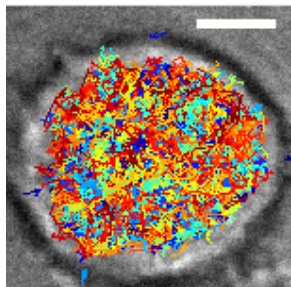
**A****B****C****D****E**

A

Stimulated

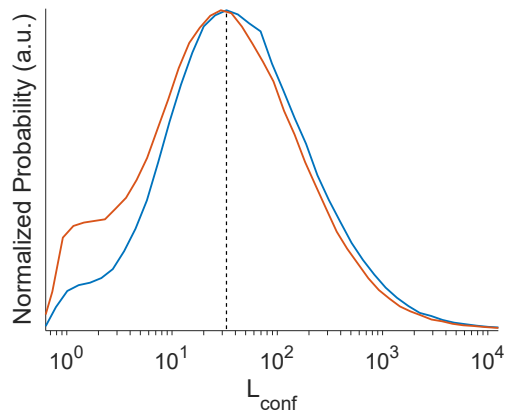


Resting

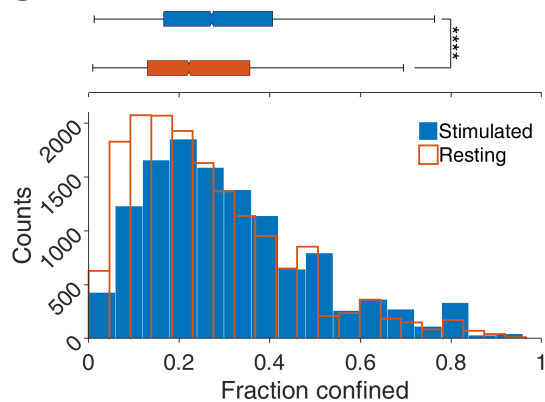


Journal Pre-proof

B

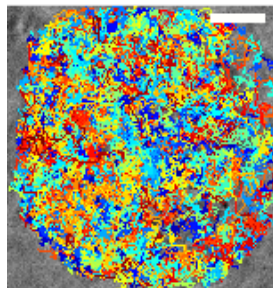


C

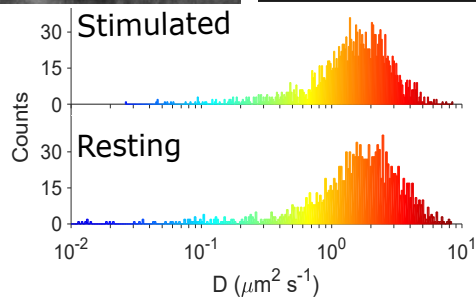
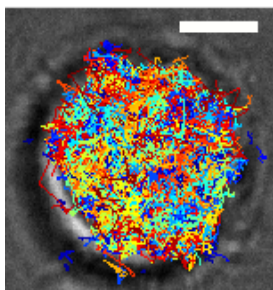


A

Stimulated

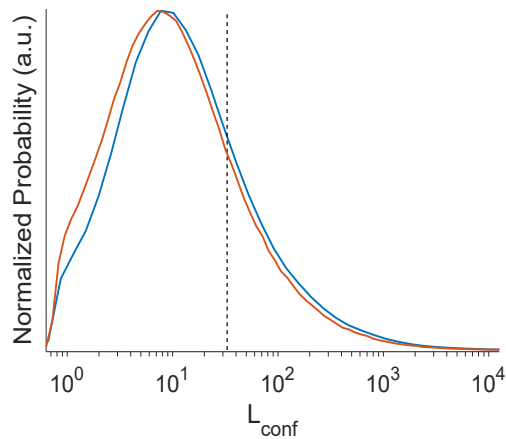


Resting

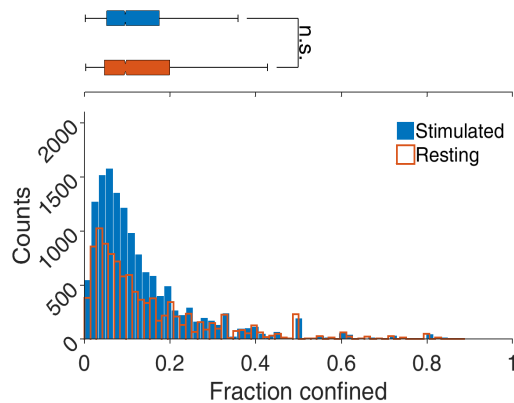


Journal Pre-proof

B



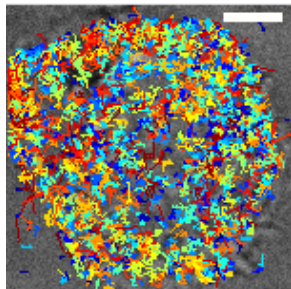
C



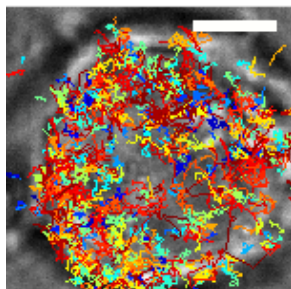


A

Stimulated

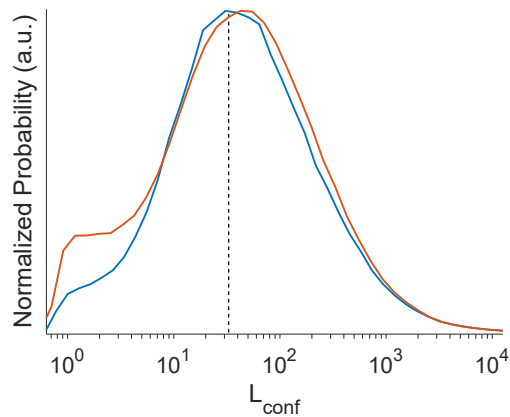


Resting

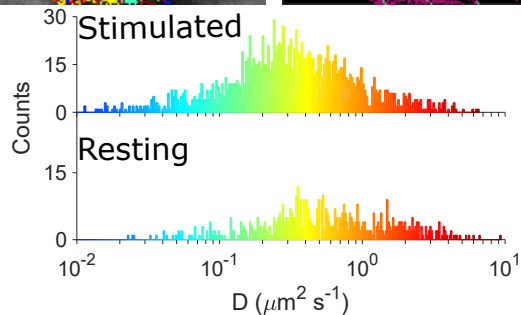
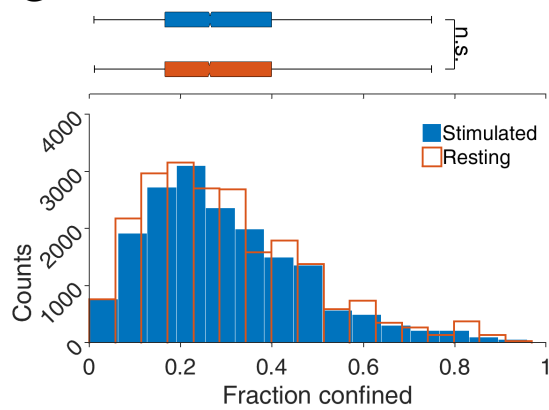


Journal Pre-proof

B

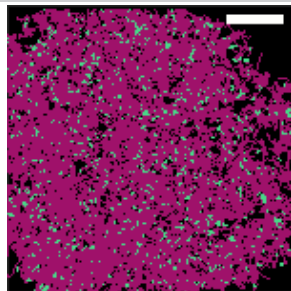
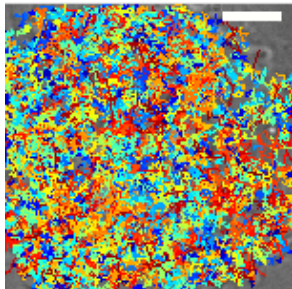


C

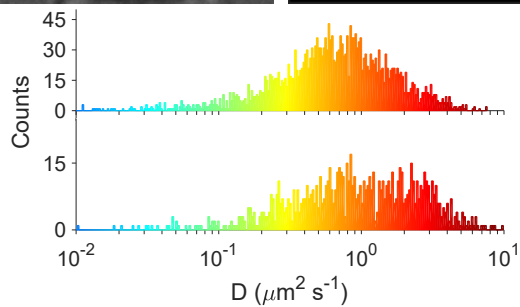
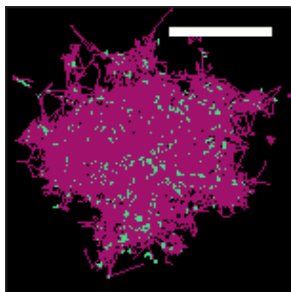
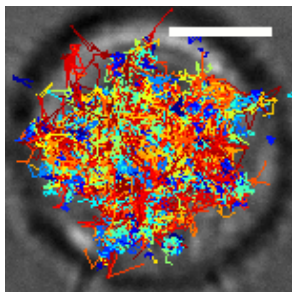


**A**

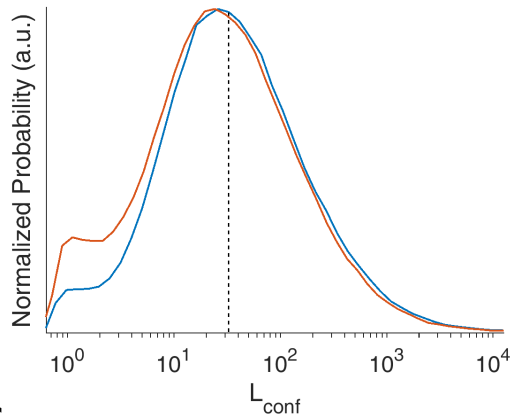
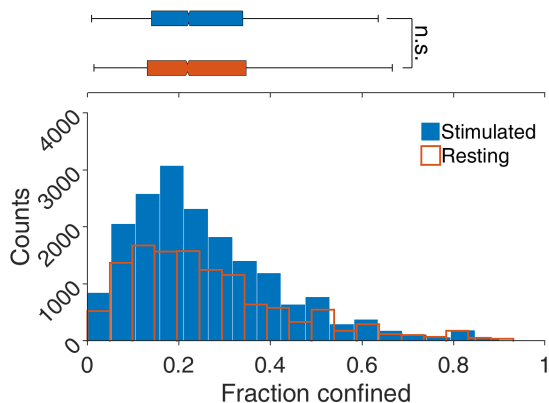
Stimulated

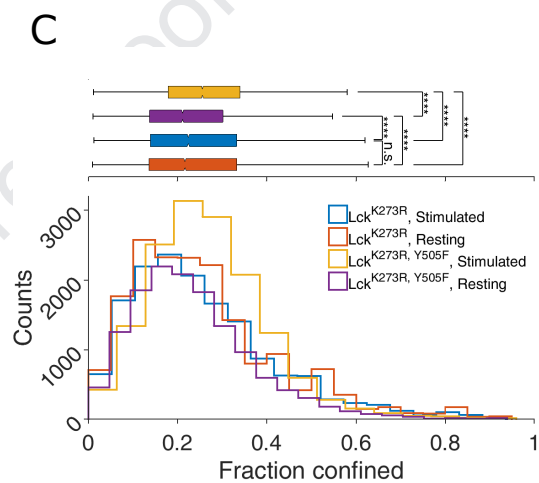
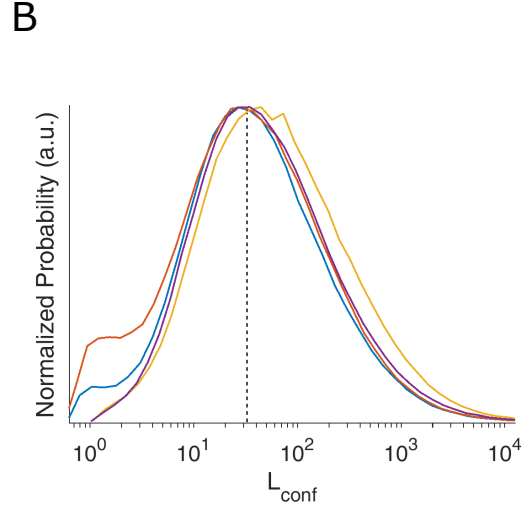
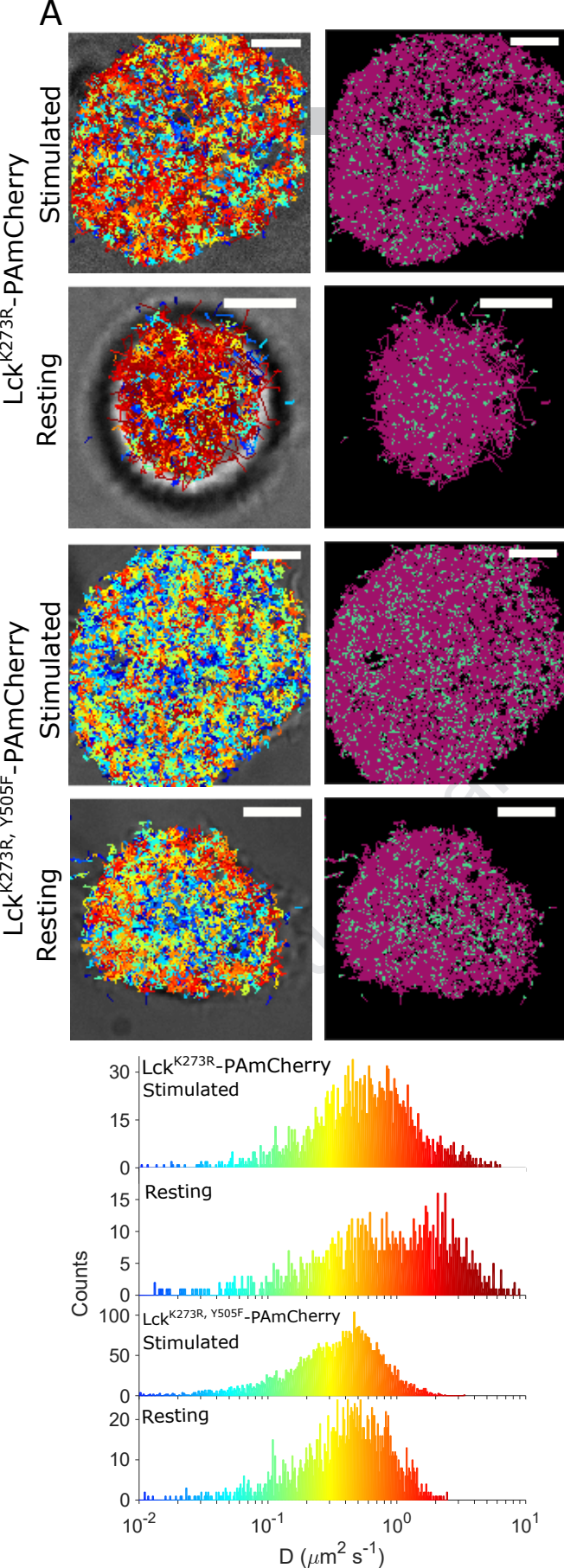


Resting

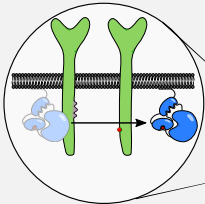


Journal Pre-proof

**B****C**



"closed" Lck



"open" Lck

